Paleoceanography and Paleoclimatology

RESEARCH ARTICLE
10.1029/2019PA003766

Rapid Loss of CO_2 From the South Pacific Ocean During the Last Glacial Termination

Katherine A. Allen[1,2], Elisabeth L. Sikes[2], Robert F. Anderson[3], and Yair Rosenthal[2]

[1]School of Earth and Climate Sciences, University of Maine, Orono, ME, USA, [2]Department of Marine and Coastal Sciences, Rutgers University, New Brunswick, NJ, USA, [3]Lamont-Doherty Earth Observatory of Columbia University, Palisades, NY, USA

Key Points:
- The southwest Pacific Ocean stored more respired CO_2 during the Last Glacial Maximum than during the Holocene
- Carbonate ion concentration of intermediate water initially increases in tandem with inferred early deglacial Southern Ocean upwelling
- Release of respired CO_2 from the interior Pacific Ocean contributed to the deglacial rise in atmospheric CO_2

Supporting Information:
- Supporting Information S1

Correspondence to:
K. A. Allen,
katherine.a.allen@maine.edu

Citation:
Allen, K. A., Sikes, E. L., Anderson, R. F., & Rosenthal, Y. (2020). Rapid loss of CO_2 from the South Pacific Ocean during the last glacial termination. *Paleoceanography and Paleoclimatology*, *35*, 2019PA003766. https://doi.org/10.1029/2019PA003766

Received 4 SEP 2019
Accepted 29 NOV 2019
Accepted article online 4 DEC 2019

Abstract During the termination of the last ice age, atmospheric CO_2 rose ~80 ppm, but the origin of this carbon has not been fully resolved. Here we present novel constraints on the patterns and processes of deglacial CO_2 release using three marine sediment cores from the southwest Pacific. Carbon isotopes ($\delta^{13}C$) and boron to calcium ratios (B/Ca) of benthic foraminiferal calcite provide records of the $\delta^{13}C$ of total dissolved inorganic carbon (DIC) and carbonate ion concentrations ($[CO_3^{2-}]$) in seawater, respectively. Together these properties indicate enhanced storage of respired CO_2 between 1.2- and 2.5-km water depth during the Last Glacial Maximum (19–23 thousand years ago, ka). The first major rise in atmospheric CO_2 during the last deglaciation, at the time of Heinrich Stadial 1, was accompanied by increases in $\delta^{13}C$ and $[CO_3^{2-}]$ at all core depths. The initial increases could be attributed to southward shifted westerly winds driving increased upwelling in the Southern Ocean, sending a signal of enhanced ventilation northward into the Pacific. Our results confirm that southern Pacific interior water masses served as an important reservoir for CO_2 during the last glacial period, likely extracted from the atmosphere via the biologic pump. Some abrupt changes in Pacific carbon storage coincide with changes in Southern Ocean pH (Rae et al., 2018, https://doi.org/10.1038/s41586-018-0614-0), upwelling indicators (Anderson et al., 2009, https://doi.org/10.1126/science.1167441), and pCO_2 (Monnin et al., 2001, https://doi.org/10.1126/science.291.5501.112), indicating that portions of the deep Pacific carbon pool can be ventilated rapidly to the atmosphere via the Southern Ocean.

1. Introduction

The Pacific Ocean fills the world's largest ocean basin and acts as a major reservoir of carbon that can be readily exchanged with the atmosphere (Key et al., 2004). Many marine geochemical paleorecords indicate that during the Last Glacial Period, the Pacific Ocean held more carbon than it does today, accounting for a substantial portion of glacial atmospheric CO_2 drawdown (Anderson et al., 2019; Basak et al., 2018; Bradtmiller et al., 2010; Hoogakker et al., 2018; Ronge et al., 2016; Sikes et al., 2016; Skinner et al., 2015). However, the amounts, specific locations, and mechanisms of glacial carbon storage and subsequent release have not been fully resolved. Some studies have examined evidence for intensified glacial carbon storage in the abyss (Basak et al., 2018; Broecker & Clark, 2010; Herguera et al., 1992; Sarnthein et al., 2013), which might be favored in an intensely salinity-stratified ocean; others have proposed the existence of a "floating," mid-depth carbon-enriched water mass sandwiched by lower carbon water (Jacobel et al., 2017; Ronge et al., 2016; Sikes, Cook, & Guilderson, 2016). Increased spatial coverage is needed to resolve the dimensions of Pacific carbon reservoirs, and independent evidence from multiple proxies is required to quantify CO_2 storage and to assess carbon sources and fluxes.

In the modern ocean, $\delta^{13}C$ of dissolved inorganic carbon ($\delta^{13}C_{DIC}$) is broadly correlated with nutrient concentrations due to the simultaneous uptake of nutrients and isotopically depleted carbon by phytoplankton in surface waters, and the release of those same nutrients and carbon when detrital, sinking organic matter is broken down by microbes in deeper waters (Broecker & Peng, 1982). South Pacific interior waters were characterized by depleted $\delta^{13}C$ during the LGM compared to the Holocene, suggesting that these waters stored more respired carbon during the glacial period (Herguera et al., 1992; Herguera et al., 2010; Sikes et al., 2016; Ullermann et al., 2016). Additional processes exert control on $\delta^{13}C_{DIC}$, and deconvolving these competing signals can be challenging even in the modern ocean (Eide et al., 2017; Gruber & Keeling, 2001; Schmittner et al., 2013). However, in the deep ocean a strong relationship exists between Apparent

Oxygen Utilization, which is the most direct measure for respired CO_2, and $\delta^{13}C_{DIC}$, demonstrating the utility of $\delta^{13}C_{DIC}$ as a means of tracking changes in respired carbon (Figure S1 in the supporting information). Additional, independent proxies may be used to complement $\delta^{13}C$ and develop a deeper understanding of marine carbon cycling. Generating independent estimates of carbonate ion concentration ($[CO_3^{2-}]$) in tandem with $\delta^{13}C_{DIC}$ is one way to gain new insight into changes in ocean carbon storage (Allen et al., 2015; Chalk et al., 2019; Marchitto et al., 2005; Yu et al., 2008; Yu et al., 2010; Yu et al., 2013).

The concentrations of carbonate ion ($[CO_3^{2-}]$) and other dissolved inorganic carbon species are governed by seawater's alkalinity and by total dissolved inorganic carbon (DIC). An injection of respired CO_2 into deep water raises DIC and initially decreases $[CO_3^{2-}]$. In turn, this lowers the saturation states of calcite and aragonite (Ω). If Ω falls far enough, seafloor carbonate deposits will begin to dissolve (Subhas et al., 2017), which releases mineral-bound calcium and carbonate ions back into seawater, raising $[CO_3^{2-}]$. Dissolution continues until a new balance between supply and loss of ingredients for carbonate is reached (Broecker & Peng, 1987).

Organic matter respiration decreases both $[CO_3^{2-}]$ and $\delta^{13}C_{DIC}$ (Yu et al., 2008). In contrast, carbonate dissolution increases $[CO_3^{2-}]$ and exerts little effect on $\delta^{13}C_{DIC}$ because the $\delta^{13}C$ of marine carbonates is very close to that of seawater (Zeebe & Wolf-Gladrow, 2001). This is one example of how $[CO_3^{2-}]$ and $\delta^{13}C_{DIC}$ may be used in concert to gain insight into specific processes affecting ocean carbon storage. Such processes include not only biologic pump activity and seafloor dissolution but also air-sea gas exchange and ocean mixing (Yu et al., 2008; Yu et al., 2019). Past $[CO_3^{2-}]$ and $\delta^{13}C_{DIC}$ may be reconstructed from the boron to calcium ratio (B/Ca) and $\delta^{13}C$, respectively, of benthic foraminiferal calcite preserved in marine sediments. Reconstructed values for bottom water oxygen may also be combined with $[CO_3^{2-}]$ to estimate past alkalinity and DIC (Anderson et al., 2019).

Our core sites in New Zealand's Bay of Plenty are well-positioned to monitor changes in deep and intermediate water masses exchanging between the Pacific and Southern Oceans (Figure 1 and Table 1). The shallowest site (1.2 km, RR0503-79 JPC, hereafter core 79) is bathed today by relatively fresh intermediate water with high $\delta^{13}C_{DIC}$ and high $[CO_3^{2-}]$. This well-ventilated, thermodynamically enriched signature is visible to ~20°N and serves as an important source of high $\delta^{13}C$ water to the ocean interior (Eide et al., 2017). The deepest site (2.5 km, RR0503-125 JPC, hereafter core 125) is influenced by a mixture of carbon-rich, lower $\delta^{13}C_{DIC}$ interior waters derived from the North Pacific and Upper Circumpolar Deep Water from the Southern Ocean. The strongest minima in $\delta^{13}C_{DIC}$ and $[CO_3^{2-}]$ in the Pacific Ocean are located at lower intermediate depth in the North Pacific (−0.6‰, 50 μmol/kg); at similar depths in the South Pacific this strong signature of organic matter respiration has been diluted by mixing with southern sourced waters. The mid-depth site lies at 1.6 km (RR0503-83 TC and JPC, hereafter core 83), below the low-salinity core of intermediate water and above the lowest-$\delta^{13}C_{DIC}$, low-oxygen core of CO_2-rich Pacific interior waters (Allen et al., 2015). Past changes in the chemical composition or extent of these water masses should be evident in these sediment records.

2. Materials and Methods

2.1. Age Control

Age models for all three cores (Table 1) were constructed using geochemically fingerprinted and previously dated tephras as well as ^{14}C ages derived from the planktic foraminifer *Globorotalia inflata* (Allen et al., 2015; Shane et al., 2006; Sikes, Elmore, et al., 2016). *G. inflata* samples were briefly sonicated in methanol, leached in 0.001N HCl, converted to CO_2, and graphitized prior to AMS-^{14}C analysis at Lawrence Livermore Center for Accelerator Mass Spectrometry. Calendar ages were calculated using INTCAL13 (Reimer et al., 2013) and ages were assigned to samples by linear interpolation (Figure 2 and Table S1 in the supporting information).

2.2. Stable Isotopes

All stable isotopes discussed in this study are derived from calcite tests of *Cibicidoides* spp., dominantly *C. wuellerstorfi*, and were previously published in Sikes, Elmore, et al. (2016). Samples were analyzed on a

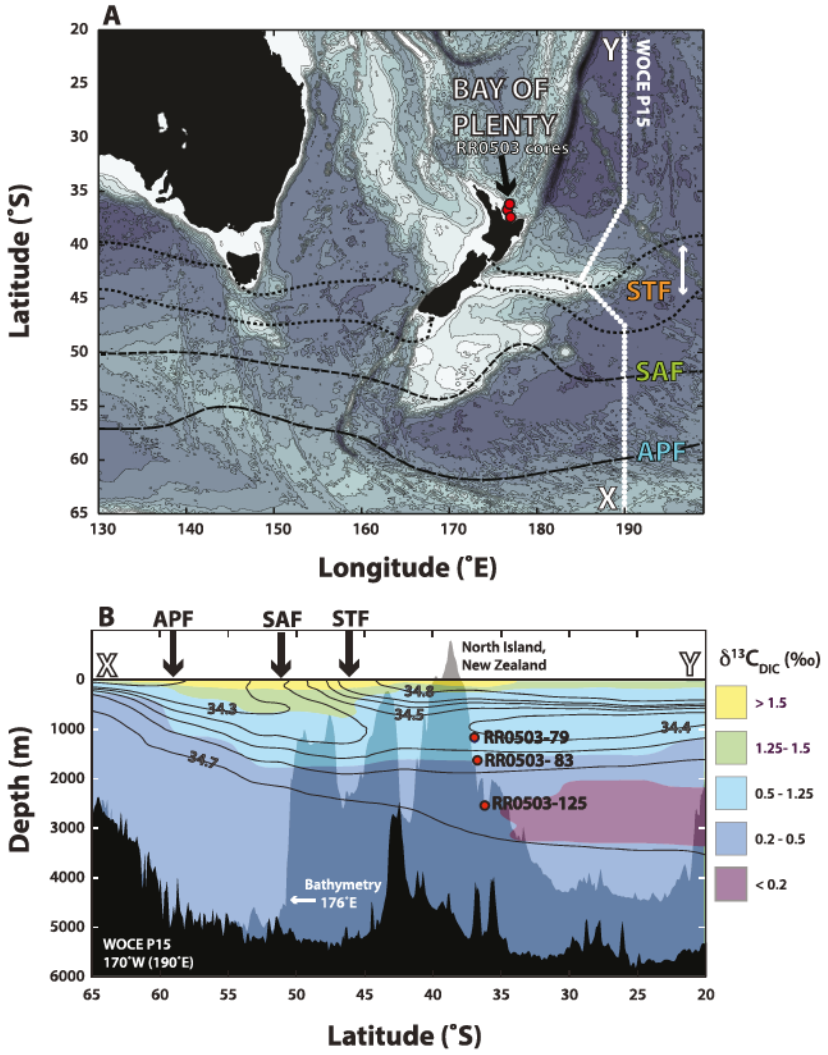

Figure 1. Study location in the southwest Pacific. (a) Sediment cores (red circles) were collected as part of a larger depth transect from New Zealand's Bay of Plenty (Sikes, Elmore, et al., 2016). The locations of the Subantarctic Front (SAF) and Antarctic Polar Front (APF) are shown in dashed lines. Two dotted lines indicate the seasonal range of the Subtropical Front (STF). (b Three sediment core sites are shown in the context of a modern water property transect (P15) from the World Ocean Circulation Experiment accessed through Ocean Data View (Key et al., 2004; Schlitzer, 2004). Salinity contours (gray) and $\delta^{13}C_{DIC}$ (colors) illustrate the influence of relatively fresh Antarctic Intermediate Water and isotopically depleted Pacific Deep/Intermediate Water.

Micromass Optima Mass Spectrometer at the Rutgers University Stable Isotope Laboratory. Further details are available in Sikes, Elmore, et al. (2016).

Table 1
Locations and Depths of Cores From the Bay of Plenty, New Zealand in the southwest Pacific

Core	Latitude (°S)	Longitude (°E)	Water depth (m)
RR0503-79	36.9585	176.5928	1165
RR0503-83	36.7375	176.6398	1627
RR0503-125	36.1983	176.8892	2541

2.3. B/Ca Sample Preparation

Sediment samples were washed through a 63-μm sieve with deionized water and then oven dried at <40 °C. *Cibicidoides wuellerstorfi* (also called *Planulina wuellerstorfi*) specimens were picked from the >150-μm size fraction (*sensu stricto*; Rae et al., 2011). Samples consisting of 5–10 specimens were partially crushed between glass slides and subjected to cleaning protocols for removal of clay particles, oxides, and organic matter (Rosenthal et al., 1997).

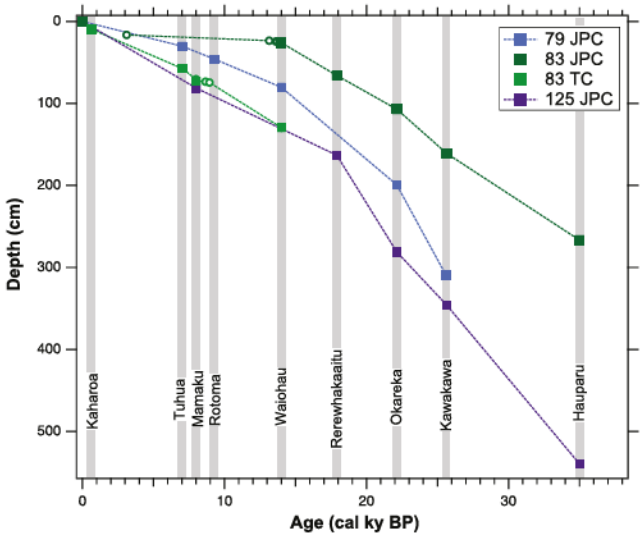

Figure 2. Age models for southwest Pacific cores based on geochemically fingerprinted tephras (squares) and planktic foraminiferal ^{14}C ages (circles). Tephrachronology is based on the work of Shane et al. (2006). Dates and depths are provided in Table S1 in the supporting information.

2.4. B/Ca Analysis

Cleaned samples were dissolved in ultrapure 0.065 N HNO_3 and analyzed on a sector-field mass spectrometer (Thermo Scientific Element XR) at Rutgers University. An aliquot of a spiked gravimetric standard was analyzed every five samples. Ammonia gas was introduced to the spray chamber to decrease boron washout times, and a suite of six standards with differing [Ca] (1.5–8 mM) was run with each batch to quantify and correct for matrix effects (Babila et al., 2014).

2.5. Carbonate Ion Calculation

Foraminiferal B/Ca values were converted to ΔCO_3^{2-} according to the modern core-top calibration of Yu et al. (2013): B/Ca = 1.14 ΔCO_3^{2-} + 176.6. Carbonate ion concentrations were then calculated from ΔCO_3^{2-} according to the equation: $\Delta CO_3^{2-} = [CO_3^{2-}]_{sat} - [CO_3^{2-}]_{in\ situ}$, where $[CO_3^{2-}]_{sat}$ is the carbonate ion concentration required for calcite saturation ($\Omega = 1$). Modern $[CO_3^{2-}]_{sat}$ values of 53.4, 58.9, and 70.6 μmol/kg were adopted for sites 79, 83, and 125, respectively, based on nearby hydrographic stations from GLODAP v2 (Olsen et al., 2016) (Table S2). Modern bottom water at 1.2 km in the southwest Pacific contains a small amount of CFC-11 and CFC-12, suggesting a maximum of ~10 μmol/kg anthropogenic CO_2 (Sabine et al., 2004; Key et al., 2004). Decreasing modern DIC by 10 μmol/kg at site 79 raises $[CO_3^{2-}]$ by 5 μmol/kg. Since the specific value of anthropogenic CO_2 at core site 79 is uncertain, and the maximum estimate falls within the 95% confidence interval of $[CO_3^{2-}]$ reconstruction here (±10 μmol/kg), a correction for anthropogenic CO_2 is not made. This should be reassessed when improved estimates of the ocean inventory of anthropogenic CO_2 are available. Bottom water at 1.6 and 2.5 km contains negligible CFC-11 (Key et al., 2004); therefore, a correction for anthropogenic CO_2 is not necessary for these sites. Youngest available samples from sites 79, 83, and 125 are 3.8, 1.4, and 0.8 ka, respectively, all predating the onset of the industrial era; $[CO_3^{2-}]$ calculated from B/Ca of *C. wuellerstorfi* from these samples according to the Yu et al. (2013) calibration falls within modern values from the southwest Pacific, with the exception of site 79 (Figure S2). This offset between the youngest sample (3.8 ka) and modern values is likely due to a real difference in $[CO_3^{2-}]$ in waters bathing this site ~4 ka compared to today. The offset does not affect downcore calculations since the full calibration equation is directly applied to fossil-derived B/Ca with no involvement of core-top values (cf., Yu et al., 2014). A uniform $[CO_3^{2-}]_{sat}$ value is assumed throughout each core because small glacial temperature, salinity, and pressure changes result in $[CO_3^{2-}]_{sat}$ differences that are within the bounds of the proxy's calibration uncertainty (Allen et al., 2015). All carbonate system calculations were done with the Matlab program CO2SYS.m (van Heuven et al., 2011) employing the total seawater scale, K_1 and K_2 constants of Lueker et al. (2000), KSO_4 of Dickson (1990), and total boron of Uppström (1974).

3. Results

3.1. Quality Control

We set minimum limits for sample Ca concentration ([Ca]) and maximum limits for levels of elements commonly present in contaminating phases (e.g., clays). Data from samples with solution [Ca] less than 0.3 mM were excluded, as were samples with Al/Ca above 1,000 μmol/mol. A total of 5 samples out of 183 were excluded on this basis (3%; see Table S3). One additional sample in core 125 was excluded due to extreme, anomalous trace element results, perhaps related to visible evidence of dissolution and an abundance of pyrite in the bulk sample. This data point will be revisited in future work involving proxies for bottom water oxygen.

Data presented in this study are derived from analyses conducted between 2011 and 2017. Recurrent analysis of the same three internal consistency standard solutions with B/Ca of 33, 160, and 239 μmol/mol yields

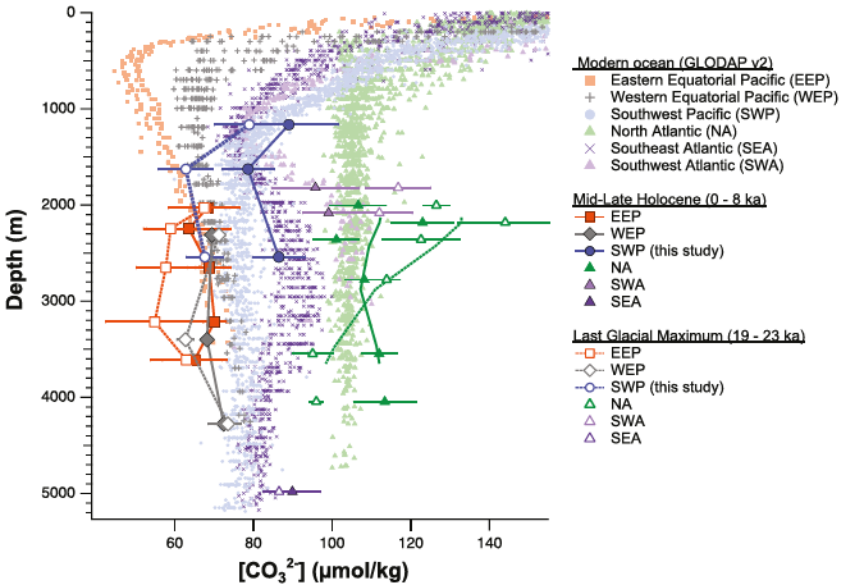

Figure 3. Comparison of mean [CO_3^{2-}] for mid-late Holocene (0–8 ka; filled symbols) and Last Glacial Maximum (LGM; 19–23 ka; open symbols). Southwest Pacific (SWP) glacial values are lower than Holocene values (blue circles; this study). In the eastern equatorial Pacific (EEP), glacial values are lower than Holocene values between ~2.2 and 3.2 km, while shallower and deeper cores have similar Holocene and LGM values (orange squares), as do those in the western equatorial Pacific (gray diamonds; Doss & Marchitto, 2013; Umling & Thunell, 2018; Yu et al., 2010; Yu et al., 2013). In the Atlantic, cores deeper than 3 km exhibit LGM [CO_3^{2-}] lower than Holocene, similar to parts of the deep Pacific. In contrast, LGM [CO_3^{2-}] in Atlantic cores shallower than 3 km is higher than Holocene values, resulting in a steeper glacial vertical [CO_3^{2-}] gradient in that ocean basin (Chalk et al., 2019; Lacerra et al., 2017; Yu et al., 2008). For most regions, Holocene averages agree with modern [CO_3^{2-}] within 1σ (horizontal bars; Key et al., 2004). Location details and average values are provided in Table S5 and Figure S3 in the supporting information.

analytical precisions of ±5.0, 2.8, and 1.9, respectively (% RSD). Corresponding standard errors are 0.5, 1.3, and 1.3 µmol/mol. Since the minimum B/Ca value in our data set is 148 µmol/mol, we apply 3% RSD.

Eight pairs of replicate samples were analyzed from core 83, which had the highest abundance of *C. wuellerstorfi*. Shells were split into two groups and crushed separately; therefore, any differences between replicates reflect both population and analytical influences. B/Ca differences between replicates ranged from 0.8 to 13.5 µmol/mol with an average of 7.5 µmol/mol (Table S4). Based on these replicate data, average standard error for reconstructed ΔCO_3^{2-} is 3.3 µmol/kg, and % RSD is 2.9, very similar to the analytical %RSD. Combining the analytical and replicate RSDs ($\sqrt{(RSD_A^2 + RSD_B^2)}$ yields 4% RSD. The standard error associated with the global B/Ca-ΔCO_3^{2-} core-top calibration is ±10 µmol/kg (Yu et al., 2013, supporting information).

3.2. Reconstructed [CO_3^{2-}] and $\delta^{13}C$ Records

Holocene [CO_3^{2-}] profiles were reconstructed from the average of available *C. wuellerstorfi* B/Ca data between 0 and 8 cal kyr B.P. for each core. The profile generated from Bay of Plenty cores (79, 83, and 125; dark blue circles) mimics modern [CO_3^{2-}] data from the region (light blue circles; Figure 3). The average Holocene value for the deepest core (125, 2.5 km) is elevated relative to modern values at the same depth. However, the youngest available value from this core (0.8 ka) agrees with modern data within 1σ (Figure S2), suggesting that the B/Ca proxy does faithfully represent bottom water conditions, and the elevated Holocene average is due to the presence of higher [CO_3^{2-}] during the early-middle Holocene.

At all three core sites in the southwest Pacific, average [CO_3^{2-}] and $\delta^{13}C$ were lower during the Last Glacial Maximum (LGM; 19–23 ka) than during the middle to late Holocene (0–8 ka) (Figures 3 and 4). At 1.2-, 1.6-, and 2.5-km depth, average glacial [CO_3^{2-}] was lower by 10, 16, and 19 µmol/kg, respectively. Based on a two-tailed Student's *t* test, the Holocene and LGM means of the two deeper cores (83 and 125) are

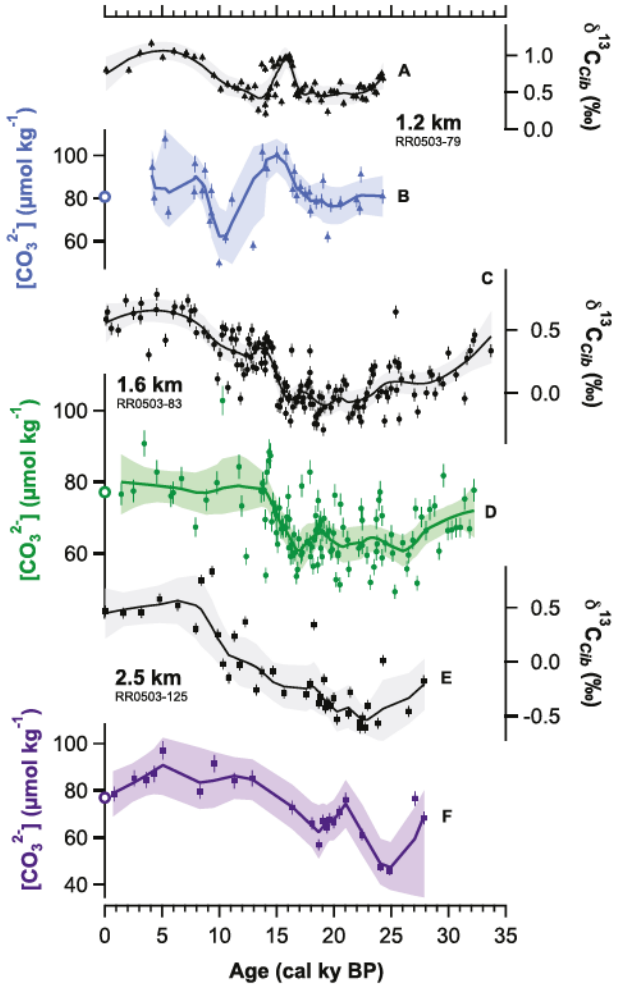

Figure 4. Carbon isotopes and $[CO_3^{2-}]$ from southwest Pacific cores for the last ~30 kyr. Isotope data (black symbols) are derived from *Cibicidoides* (Sikes, Elmore, et al., 2016) and $[CO_3^{2-}]$ estimates (colored symbols) are derived from *C. wuellerstorfi* B/Ca according to the calibration of Yu et al. (2013). Vertical error bars on individual data points are ±0.05‰ for isotopes (1σ precision of standards) and ±4% for $[CO_3^{2-}]$ (combined analytical and population-variation RSD; see text for details). Solid lines represent the average of 1,000 smoothed Monte Carlo simulations of the data resampled within ±10 μmol/kg and ±0.25‰ for $[CO_3^{2-}]$ and $\delta^{13}C$, respectively. Shaded bands represent the nonparametric 95% confidence interval for the smoothed mean (see supporting information for details). Open symbols located at zero age represent the modern bottom water $[CO_3^{2-}]$ at core sites.

significantly different at a >99% confidence level, while those for the shallowest core (79) are different at an 89% confidence level.

The initial deglacial rise in both $\delta^{13}C$ and $[CO_3^{2-}]$ in all cores occurs within Heinrich Stadial 1 (~18.0–14.5 ka). Assigning a more precise timing for these changes is not currently possible given the combined uncertainties of the age model and the proxy-based reconstructions and the strong variability within each record, particularly in core 83 (supporting information). In all three cores, $\delta^{13}C$ and $[CO_3^{2-}]$ roughly covary throughout the records, with the exception of core 79 from ~12 to 8 ka (Figure 4).

Interior waters experience minima in both $\delta^{13}C$ and $[CO_3^{2-}]$ during the glacial period, with lowest values occurring below 1.5 km (Figure 5). During the deglaciation, both $\delta^{13}C$ and $[CO_3^{2-}]$ rise slowly in deep water (2.5 km) and increase in rapid steps in mid-depth and shallow water (<2 km; Figures 4 and 5). Average Holocene and LGM $\delta^{13}C$ and $[CO_3^{2-}]$ for all three southwest Pacific cores are also shown on a $\delta^{13}C$ versus $[CO_3^{2-}]$ cross-plot (Figure 6). The mean LGM to Holocene trajectories in $\delta^{13}C$ versus $[CO_3^{2-}]$ space for all three cores are remarkably similar considering the wide depth range (1.2–2.5-km water depth) and the different deglacial evolutions of each core (Figure 4).

4. Discussion

4.1. Last Glacial Maximum in the Southwest Pacific

At all three core sites, average $[CO_3^{2-}]$ and $\delta^{13}C$ were lower during the LGM (19–23 ka) than during the middle to late Holocene (0–8 ka; Figures 3 and 4). At 1.2-, 1.6-, and 2.5-km depth, average glacial $[CO_3^{2-}]$ was lower by 10, 16, and 19 μmol/kg, respectively, and these Holocene and LGM means are significantly different at 89% (1.2 km) and >99% confidence levels (1.6 and 2.5 km; two-tailed Student's *t* test). Given that glacial surface ocean $[CO_3^{2-}]$ was likely elevated ~50 μmol/kg relative to the Holocene (Barker & Elderfield, 2002; Lea et al., 1999), the surface-to-interior ocean differences in this region must have been 60-70 μmol/kg greater during the LGM than during the Holocene, consistent with the idea of higher biologic pump efficiency during the glacial period (Allen et al., 2015; Anderson et al., 2019; Hertzberg et al., 2016; Sikes, Elmore, et al., 2016).

The biologic pump dominates the modern deep-ocean distributions of $\delta^{13}C$ (Craig, 1970; Kroopnick, 1985; Lynch-Stieglitz et al., 1995) and $[CO_3^{2-}]$ (Yu et al., 2008). If we assume that the entire glacial-interglacial $\delta^{13}C$ change at these sites is due to degradation of biogenic material, and that isotopic compositions and stoichiometric ratios of those materials remained roughly the same as today, the expected mean glacial $[CO_3^{2-}]$ at site 83 due to the addition of respiratory CO_2 is calculated to be ~70 μmol/kg (assuming $\delta^{13}C$ of organic matter is −24‰, $\delta^{13}C$ of dissolving carbonate is 0‰, and C_{org}:C_{CaCO3} of regenerated material above the lysocline in the Pacific is 1.3 after Broecker and Sutherland (2000)). Any discrepancy between such a simplistic prediction and a measured value could be explained by a number of factors, including changes in the isotopic or stoichiometric composition of biogenic particles, the ratio of organic matter to carbonate in degrading material, formation/dissolution of marine carbonates, including the global increase in ocean alkalinity during the LGM due to carbonate compensation, the temperature or extent of air-sea $\delta^{13}C$ equilibration, and/or kinetic effects. Our rough estimate of 70 μmol/kg based solely on $\delta^{13}C$ is 7 μmol/kg higher than the value of 63 μmol/kg reconstructed from B/Ca for this site (Table S5), which is within the calibration uncertainty reported by Yu and Elderfield (2007).

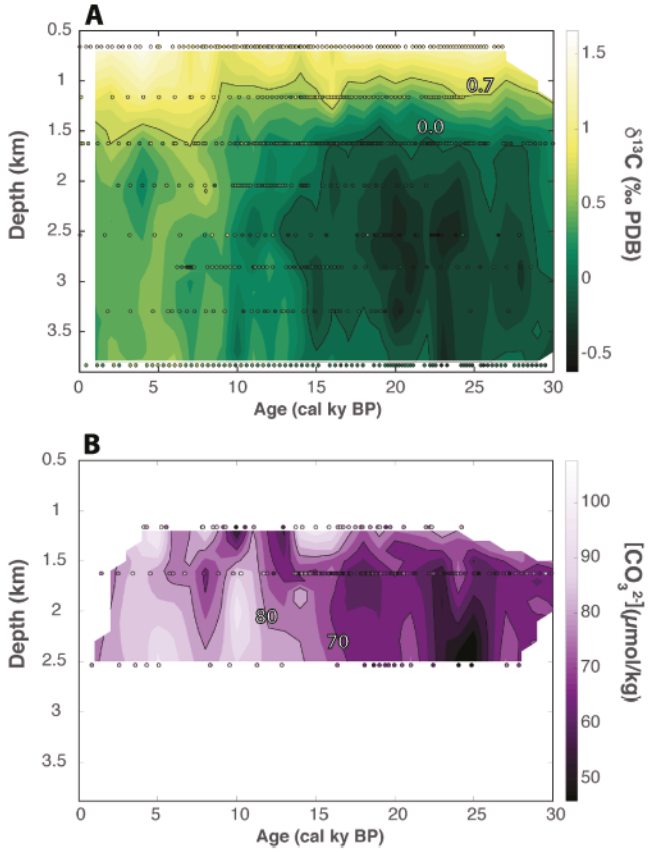

Figure 5. Depth versus age contour plot of $\delta^{13}C$ and $[CO_3^{2-}]$ data shown in Figure 4 and from Sikes, Elmore, et al. (2016). Colored dots represent individual data points (Table S3); color contours are drawn at 0.1‰ and 5-μmol/kg intervals in (a) and (b), respectively. During the glacial period, low-$\delta^{13}C$ and low-$[CO_3^{2-}]$ water exists below 1.5-km water depth. Both $\delta^{13}C$ and $[CO_3^{2-}]$ increase during the glacial termination, achieving near-modern values by the mid-Holocene.

The glacial-interglacial trajectories of all three southwest Pacific cores roughly align with the best fit photosynthesis-respiration line for the modern ocean from Yu et al. (2008), implying that, like today, the degradation of sinking biogenic particles played a dominant role in setting the $[CO_3^{2-}]$ and $\delta^{13}C$ of the glacial ocean (Figure 6). Radiocarbon evidence suggests that much of the deep ocean (>2 km) had higher reservoir ages and was less well ventilated during the last glacial period than today, perhaps accounting for nearly half of the glacial-interglacial CO_2 change (Sarnthein et al., 2013; Sikes, Cook, & Guilderson, 2016; Skinner et al., 2015). At some locations in the North and South Atlantic, benthic $\delta^{13}C$ closely follows the pattern of $\delta^{13}C$ of atmospheric CO_2, implying that a portion of these records may be explained by partial equilibration with a ^{13}C-depleted atmosphere (Lund et al., 2019; Lynch-Stieglitz et al., 2019); in contrast, our southwest Pacific records do not emulate atmospheric composition during the early deglaciation, implying stronger influence of oceanic processes in the Pacific. Although the overall trend in the relationship between $\delta^{13}C$ and $[CO_3^{2-}]$ during the LGM is consistent with greater storage of respiratory CO_2 in deep water, sufficient variability exists within the records to allow for imprints from other processes, such as air-sea gas exchange. Additional reconstructions for dissolved nutrients (Yu et al., 2019) and/or oxygen (Anderson et al., 2019) are needed to quantify specific carbon contributions from carbonate dissolution, organic matter respiration, and air-sea gas exchange.

4.2. Last Glacial Maximum in the Pacific Versus Atlantic

In the Atlantic Ocean, the LGM is characterized by a steeper vertical $[CO_3^{2-}]$ gradient (shallow-to-deep difference) than in the Holocene, with higher $[CO_3^{2-}]$ above 2.5 km and lower $[CO_3^{2-}]$ below 3 km, consistent with the idea of a relatively well ventilated upper cell and poorly ventilated deep water during that time (Chalk et al., 2019; Lund et al., 2015; Yu et al., 2008). In contrast, our South Pacific results indicate lower $[CO_3^{2-}]$ between 1.2 and 2.5 km (Figure 3), supporting the idea that mid-depth waters in this region were relatively isolated from the atmosphere and able to accumulate respired CO_2 from sinking biologic detritus (Ronge et al., 2016; Sikes et al., 2000; Sikes, Cook, & Guilderson, 2016; Skinner et al., 2015).

In the western equatorial Pacific, LGM-Holocene $[CO_3^{2-}]$ offsets are typically small (3–5 μmol/kg), interpreted to reflect efficient pH buffering by dissolution of seafloor carbonates to compensate for greater storage of respiratory CO_2 (Umling & Thunell, 2018; Yu et al., 2013). Offsets in the south Pacific (this study) and eastern equatorial Pacific (Doss & Marchitto, 2013; Umling & Thunell, 2018) are larger (~10–20 μmol/kg), perhaps because these sites remained above the lysocline and/or experienced an ongoing injection of CO_2 that outpaced $CaCO_3$ dissolution.

During the LGM, $[CO_3^{2-}]$ estimates for the deep Atlantic and Pacific lie closer together than they do during the Holocene, while the opposite is true for the shallow Atlantic (above 3 km) (Figure 3). Together with stable isotope data, this supports the idea that communication between Atlantic and Pacific basins via the Southern Ocean was reduced for shallower waters during the LGM, effectively isolating the shallow Atlantic overturning cell from the rest of the ocean (Ferrari et al., 2014; Sikes et al., 2017).

4.3. Deglaciation

The end of the last ice age was marked by a rapid rise in atmospheric CO_2 accompanied by abrupt changes in the Southern Hemisphere, including increased upwelling and rising deep-water pH in the Southern Ocean (Anderson et al., 2009; Rae et al., 2018). The sharp rise in atmospheric temperature at midlatitudes in the Southern Hemisphere prior to a major rise in CO_2 (Putnam et al., 2013) suggests an abrupt southward shift of the westerly winds, which could have driven a breakdown in glacial stratification and a release of CO_2

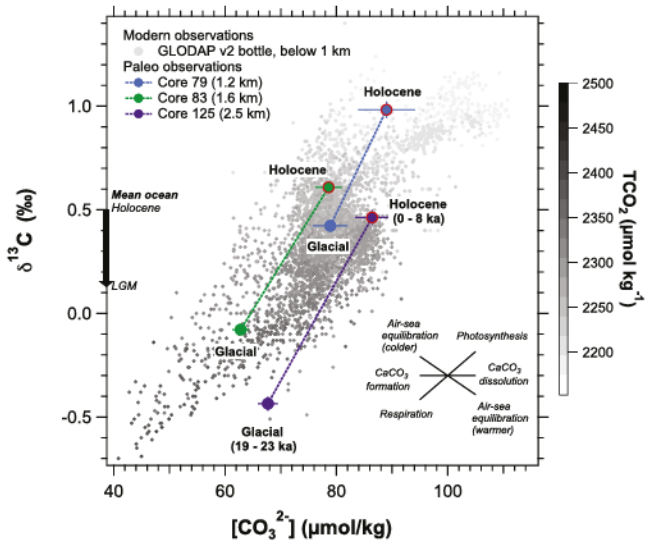

Figure 6. Comparison of mean $\delta^{13}C$ and $[CO_3^{2-}]$ in the southwest Pacific for mid-late Holocene (0–8 ka) and glacial (19–2 ka) intervals. At all three core sites, both $\delta^{13}C$ and $[CO_3^{2-}]$ are lower during the glacial period. Error bars represent standard error of the mean. Gray-scale dots are from the global data set of Schmittner et al. (2013); only data >1 km are shown, and $[CO_3^{2-}]$ was calculated from published alkalinity, DIC, salinity, temperature, phosphate, and silicate data. The mean ocean shift (black arrow on *y* axis) of 0.34‰ is from Peterson et al. (2014). The slope of photosynthesis-respiration line is the best fit for modern deep water from Yu et al. (2008), the $CaCO_3$ line assumes that $\delta^{13}C$ of marine carbonate and seawater are equal, and the air-sea slope was calculated assuming 0.1‰ enrichment of DIC per °C of cooling (Lynch-Stieglitz et al., 1995; Mook et al., 1974) and allowing full equilibration (see supporting information).

from the ocean (Toggweiler & Russell, 2008). Such an atmospheric shift has the potential to affect a wide region, spanning the full breadth of the Southern Ocean including intermediate and deep water formation regions.

At site 79 (1.2-km water depth) in the South Pacific, $[CO_3^{2-}]$ and $\delta^{13}C$ start to rise ~18 ka, at the start of HS1 (Figure 4). This shift occurs at the same time as the first deglacial pulse of upwelling in the Southern Ocean (Anderson et al., 2009) and a sharp increase in $\delta^{13}C$ at the same depth in the southwest Atlantic (Lund et al., 2015; Sikes et al., 2017; Figure S4). Today, low-salinity intermediate water interacts with the atmosphere at high latitudes and then sinks before moving to lower latitudes, carrying a signature of Southern Ocean air-sea gas exchange northward. Therefore, the paired rise in $[CO_3^{2-}]$ and $\delta^{13}C$ at site 79 is consistent with a deepening of the boundary between well-ventilated intermediate waters and more poorly ventilated deep water during this time (Clementi & Sikes, 2019; Pahnke & Zahn, 2005; Ronge et al., 2015), and extends the footprint of wind-driven ventilation into the midlatitude Pacific.

The strong positive excursion in both $[CO_3^{2-}]$ and $\delta^{13}C$ (~18–15 ka) is contrary to the global pattern of $\delta^{13}C$ of atmospheric CO_2 (Schmitt et al., 2012), suggesting that gas exchange with the atmosphere is not able to strongly overprint or fully reset the oceanic $\delta^{13}C$ signal at this Pacific site during HS1, in contrast to some Atlantic sites (Lund et al., 2019; Lynch-Stieglitz et al., 2019). Later in the deglaciation, from ~12 to 8 ka, $[CO_3^{2-}]$ decreases while $\delta^{13}C$ increases at site 79. This temporary decoupling of $[CO_3^{2-}]$ and $\delta^{13}C$ suggests the influence of a process other than the creation or destruction of organic matter. One way to achieve such a decoupling in the modern ocean is to lower the temperature at which air-sea gas exchange occurs and allow partial or full re-equilibration (Lynch-Stieglitz et al., 1995). However, oxygen isotope data from core 79 (Sikes, Elmore, et al., 2016) are not consistent with a cooling of intermediate water at this time. Alternatively, it is possible that $\delta^{13}C$ rose and $[CO_3^{2-}]$ fell due to a change in the nature of air-sea gas exchange between 12 and 8 ka. During this interval, atmospheric pCO_2 was rising and the $\delta^{13}C$ of atmospheric CO was also increasing (Schmitt et al., 2012). Invasion of relatively $\delta^{13}C$-enriched atmospheric CO_2 into Southern Ocean surface water could have resulted in isotopically enriched, lower $[CO_3^{2-}]$ surface water that was eventually transformed to Antarctic Intermediate Water near the Polar Front, bringing this signal northward into the southwest Pacific. Independent temperature and nutrient reconstructions are needed to assess these possibilities.

Bottom water $[CO_3^{2-}]$ at sites 83 (1.6 km) and 125 (2.5 km) begins to rise ~18 ka as well, and $[CO_3^{2-}]$ at all three core sites continues to rise through HS1. What mechanism(s) could account for a rise in deep $[CO_3^{2-}]$ at this time? Today sites 83 and 125 are both strongly influenced by Circumpolar Deep Water (CDW). CDW represents a mixture derived from North Atlantic Deep Water, Pacific Deep Water, and Indian Deep Water. In addition, Antarctic shelf water that is not dense enough to become bottom water becomes part of CDW (e.g., Weddell Sea Deep Water; Talley, 2011). Therefore, the properties of CDW may be affected by changing the properties of one or more of these component water masses and/or by altering the mixing proportions. Today sites 83 and 125 fall within a local oxygen minimum, indicating the presence of Upper Circumpolar Deep Water dominated by Pacific Deep Water and Indian Deep Water contributions, as opposed to Lower Circumpolar Deep Water, which is identified by higher salinity caused by a stronger contribution from North Atlantic Deep Water (Orsi et al., 1999). A deglacial increase in $[CO_3^{2-}]$ of Upper Circumpolar Deep Water in the southwest Pacific could be driven by (1) an increase in $[CO_3^{2-}]$ of Pacific Deep Water and/or Indian Deep Water, (2) a relative increase in the proportion of Atlantic-sourced or Antarctic-sourced deep water characterized by relatively higher $[CO_3^{2-}]$, and/or (3) loss of respired CO_2 by increased ventilation to the atmosphere.

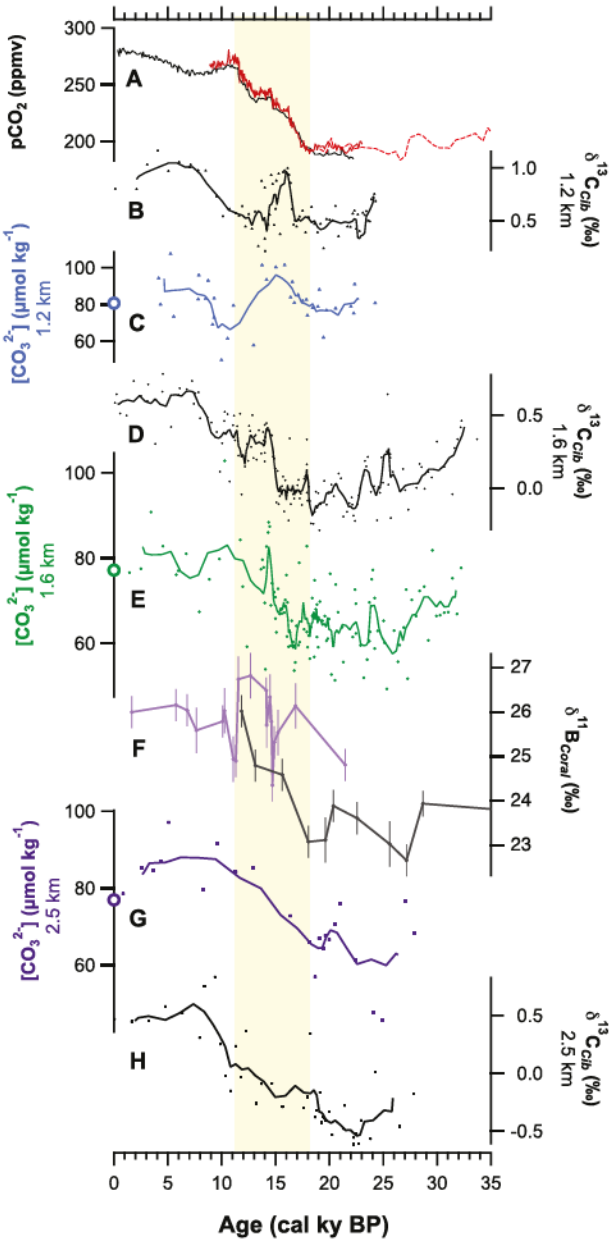

Figure 7. Comparison of marine and atmospheric records of the last deglaciation. (a) Atmospheric CO_2 from Monnin (2001) (black line), Marcott (2014) (red line), and Ahn and Brook (2008) (dashed line). (b and c) Benthic $\delta^{13}C$ and $[CO_3^{2-}]$ from core 79. (d and e) $\delta^{13}C$ and $[CO_3^{2-}]$ from core 83. (f) Boron isotopes from deep-sea corals in Drake Passage (Rae et al., 2018), where black line = "deep cell" and purple = "upper cell" (see text for details). (g and h) $\delta^{13}C$ and $[CO_3^{2-}]$ from core 125. Lines in (b)–(e), (g), and (h) represent 5-point running means. Open symbols on the *y* axes at zero age represent modern bottom water composition.

In the Pacific, glacial $[CO_3^{2-}]$ is similar to Holocene values in the western and equatorial Pacific (Figure 3), indicating that a large portion of the deep Pacific was characterized by stable $[CO_3^{2-}]$. This suggests that an increase in the relative influence of higher-$[CO_3^{2-}]$ water masses is a more likely explanation. Independent εNd evidence from the South Atlantic and southwest Pacific point to enhanced input of more isotopically depleted North Atlantic-sourced water to the South Pacific during deglaciations (Hu et al., 2016), consistent with this mechanism. To develop a deeper understanding of the potential contributions of different water masses to deep-ocean $[CO_3^{2-}]$ change in the southwest Pacific, more data are needed to assess glacial-interglacial $[CO_3^{2-}]$ in the North Pacific, Indian, and Southern Oceans.

The biological pump was more efficient during the last glacial period than it is todday (Martínez-García et al., 2014; Studer et al., 2015). A deglacial decrease in the efficiency of the global biological pump could account for a portion of deglacial atmospheric CO_2 rise and also drive an increase in interior-ocean $[CO_3^{2-}]$ (Lacerra et al., 2019), potentially accounting for portions of deglacial $[CO_3^{2-}]$ rise in our southwest Pacific records. A decrease in biological pump efficiency corresponds to a less complete utilization of nutrients in the surface ocean (Knox & McElroy 1984). Therefore, in the absence of changes in ocean circulation, a decrease in efficiency is expected to drive a decrease in total export production out of the surface mixed layer, with decreasing impact at greater depths following a flux attenuation curve (Martin et al., 1987). Given the variability and resolution of our data set, assessing relatively short, millennial-scale changes on the order of HS1 is challenging; a comparison of glacial versus interglacial $[CO_3^{2-}]$ averages is more robust. Within our three-core depth transect, the glacial-interglacial $[CO_3^{2-}]$ difference *increases* with depth: 10 μmol/kg (1.2 km), 15 μmol/kg (1.6 km), and 19 μmol/kg (2.5 km). These observations are contrary to predictions based on decreased biologic pump efficiency occurring in the absence of a change in ocean ventilation. Instead, the observations point to an important role for ocean physics in driving the deglacial change in biologic pump efficiency. The increasing magnitude of glacial-interglacial $[CO_3^{2-}]$ difference with depth (Figure 3) suggests that the greatest change in ventilation within our transect occurred at 2.5 km, with smaller changes in ventilation occurring at shallower depths, pointing to a glacial-interglacial change in ocean circulation.

Support for a Southern Ocean link is provided by concurrent changes in Southern Ocean pH (Figure 7; Rae et al., 2018). In the absence of competing effects, an increase in CO_2 content of seawater results in a decrease in pH. The existence of a strong horizontal pH gradient in the Drake Passage during the LGM suggests relative carbon enrichment of deeper Pacific water, while the breakdown of that gradient during deglaciation suggests ventilation—a transfer of carbon from the deep ocean to the upper ocean (Rae et al., 2018). The deglacial rise in pH of the Southern Ocean "lower cell" is matched by the $[CO_3^{2-}]$ and $\delta^{13}C$ rise at South Pacific site 125 (Figure 7), pointing to deglacial ventilation of the South Pacific via the Southern Ocean.

Today the South Pacific sites (79, 83, and 125) and Drake Passage sites (Rae et al., 2018) are characterized by similar neutral density, and modern dissolved oxygen transects reveal a distinct low-oxygen core of Pacific Deep Water penetrating the Southern Ocean at Drake Passage (Figure S6), consistent with the idea that these Drake Passage depths are fed by South Pacific sources (Reid, 1997). Our results suggest that deeply

sequestered CO_2 was released not only from the Southern Ocean at this time (~6% of modern ocean volume) but also from the interior South Pacific as well (~24% of modern ocean volume; Peterson et al., 2014), ultimately tapping a larger reservoir of carbon. The alignment of both millennial-scale and longer-term shifts in $[CO_3^{2-}]$ and $\delta^{13}C$ at our two deeper sites with pH excursions in the Drake Passage suggests that, like today, the Southern Ocean was a major conduit for global-scale ocean-atmosphere gas exchange.

These observations of rising $[CO_3^{2-}]$ and pH are inconsistent with predictions for major release of geologic CO_2 to the deep ocean during the deglaciation (Stott et al., 2019). An injection of mantle-derived CO_2 into seawater would cause an immediate decrease in $[CO_3^{2-}]$ and pH, contrary to observations. Our results do not preclude the possibility of some amount of mantle-derived CO_2 entering the atmosphere via a different region (e.g., in the EEP), but they do provide evidence for a deglacial loss of CO_2 from a large portion of the Pacific dominated by respired carbon rather than geologic carbon.

5. Conclusions

1. In the southwest Pacific between 1.2- and 2.5-km water depth, average $[CO_3^{2-}]$ was lower during the LGM than during the Holocene. Previous work has shown that $[CO_3^{2-}]$ of surface water was at least 50 μmol/kg greater during the LGM. Thus, the new results indicate much stronger vertical gradients (surface to mid-depth) of $[CO_3^{2-}]$ during the LGM compared to the Holocene.

2. During the LGM, water masses in the Atlantic and Pacific shallower than 3 km were characterized by larger interbasinal $[CO_3^{2-}]$ contrasts (~50 μmol/kg) than during the Holocene (~20 μmol/kg). Interbasinal $[CO_3^{2-}]$ contrasts in deeper waters (>3 km) were smaller.

3. Deglacial trends roughly align with the $[CO_3^{2-}]$-$\delta^{13}C$ slope predicted for modern regenerated biogenic material, implying a dominant role for the biologic pump in sequestering glacial CO_2 in the South Pacific. Additional nutrient and/or dissolved oxygen records are needed to isolate competing effects on $[CO_3^{2-}]$ and $\delta^{13}C$.

4. During the deglaciation, $[CO_3^{2-}]$ in all three cores begins to rise ~18 cal kyr B.P. and continues to rise through 15 cal kyr B.P, consistent with increasing ventilation of deep water associated with a southward displacement of the southern westerlies.

5. Today, mid-atmosphere temperature contrasts have increased, strengthening westerly winds (Swart & Fyfe, 2012; Toggweiler & Russell, 2008). If enhanced modern wind-driven mixing more effectively taps the modern deep-ocean carbon reservoir, it could make the Pacific Ocean a less effective sink for anthropogenic CO_2 (Tamsitt et al., 2017). Our results suggest that this scenario has already played out during the last glacial termination. Further work is needed to quantify the amounts and rates of carbon release that are possible via these mechanisms.

Acknowledgments
This research was supported by the NOAA Climate & Global Change Postdoctoral Fellowship Program, administered by the University Corporation for Atmospheric Research (K. Allen). Support was also provided by NSF OCE-0823487 (E. Sikes) and a Hanse-Wissenschaftskolleg Twin Fellowship (K. Allen). Many thanks to Amanda Williams, Kristine Babyak, Cassandre Stirpe, and Kaixuan Bu for their assistance in the laboratory at Rutgers. Thanks also to Aaron Putnam at the University of Maine, Thomas Guilderson at Lawrence Livermore National Laboratory, and Joellen Russell at the University of Arizona for their insightful discussions. Special thanks to Bill Halteman at the University of Maine for the guidance on statistical analysis. Upon publication, data from this study will be made publicly available at NOAA's National Centers for Environmental Information (https://www.ncei.noaa.gov/).

References

Ahn, J., & Brook, E. J. (2008). Atmospheric CO_2 and climate on millennial time scales during the last glacial period. *Science*, *322*(5898), 83–85. https://doi.org/10.1126/science.1160832

Allen, K. A., Sikes, E. L., Honisch, B., Elmore, A. C., Guilderson, T. P., Rosenthal, Y., & Anderson, R. F. (2015). Southwest Pacific deep water carbonate chemistry linked to high southern latitude climate and atmospheric CO_2 during the Last Glacial Termination. *Quaternary Science Reviews*, *122*, 180–191.

Anderson, R. F., Ali, S., Bradtmiller, L. I., Nielsen, S. H. H., Fleisher, M. Q., Anderson, B. E., & Burckle, L. H. (2009). Wind-driven upwelling in the Southern Ocean and the deglacial rise in atmospheric CO_2. *Science*, *323*, 1443–1448. https://doi.org/10.1126/science.1167441

Anderson, R. F., Sachs, J. P., Fleisher, M. Q., Allen, K. A., Yu, J. M., Koutavas, A., & Jaccard, S. L. (2019). Deep-sea oxygen depletion and ocean carbon sequestration during the Last Ice Age. *Global Biogeochemical Cycles*, *33*, 301–317. https://doi.org/10.1029/2018GB006049

Babila, T. L., Rosenthal, Y., & Conte, M. H. (2014). Evaluation of the biogeochemical controls on B/Ca of *Globigerinoides ruber* white from the Oceanic Flux Program, Bermuda. *Earth and Planetary Science Letters*, *404*, 67–76.

Barker, S., & Elderfield, H. (2002). Foraminiferal calcification response to glacial-interglacial changes in atmospheric CO_2. *Science*, *297*(5582), 833–836. https://doi.org/10.1126/science.1072815

Basak, C., Fröllje, H., Lamy, F., Gersonde, R., Benz, V., Anderson, R. F., et al. (2018). Breakup of last glacial deep stratification in the South Pacific. *Science*, *359*(6378), 900–904. https://doi.org/10.1126/science.aao2473

Bradtmiller, L. I., Anderson, R. F., Sachs, J. P., & Fleisher, M. Q. (2010). A deeper respired carbon pool in the glacial equatorial Pacific Ocean. *Earth and Planetary Science Letters*, *299*, 417–425.

Broecker, W., & Clark, E. (2010). Search for a glacial-age C-14-depleted ocean reservoir. *Geophysical Research Letters*, *37*, L13606. https://doi.org/10.1029/2010GL043969

Broecker, W., and T. Peng, 1982: Tracers in the Sea. Lamont-Doherty Geological Observatory.

Broecker, W. S., & Peng, T. H. (1987). The role of $CaCO_3$ compensation in the glacial to interglacial atmospheric CO_2 change. *Global Biogeochemical Cycles*, *1*, 15–29.

Broecker, W. S., & Sutherland, S. (2000). Distribution of carbonate ion in the deep ocean: Support for a post-Little Ice Age change in Southern Ocean ventilation? *Geochemistry, Geophysics, Geosystems*, *1*(7). https://doi.org/10.1029/2000GC000039

Chalk, T. B., Foster, G. L., & Wilson, P. A. (2019). Dynamic storage of glacial CO_2 in the Atlantic Ocean revealed by boron [CO_3^{2-}] and pH records. *Earth and Planetary Science Letters*, *510*, 1–11.

Clementi, V. J., & Sikes, E. L. (2019). Southwest Pacific vertical structure influences on oceanic carbon storage since the Last Glacial Maximum. *Paleoceanography and Paleoclimatology*, *34*, 734–754.

Craig, H. (1970). Abyssal carbon 13 in the South Pacific. *Journal of Geophysical Research*, *75*, 691–695.

Dickson, A. G. (1990). Thermodynamics of the dissociation of boric acid in synthetic seawater from 273.15 to 318.15 K. *Deep Sea Research*, *37*, 755–766.

Doss, W., & Marchitto, T. M. (2013). Glacial deep ocean sequestration of CO_2 driven by the eastern equatorial Pacific biologic pump. *Earth and Planetary Science Letters*, *377*, 43–54.

Eide, M., Olsen, A., Ninnemann, U. S., & Johannessen, T. (2017). A global ocean climatology of preindustrial and modern ocean delta C-13. *Global Biogeochemical Cycles*, *31*, 515–534. https://doi.org/10.1002/2016GB005473

Ferrari, R., Jansen, M. F., Adkins, J. F., Burke, A., Stewart, A. L., & Thompson, A. F. (2014). Antarctic sea ice control on ocean circulation in present and glacial climates. *Proceedings of the National Academy of Sciences of the United States of America*, *111*, 8753–8758.

Gruber, N., & Keeling, C. D. (2001). An improved estimate of the isotopic air-sea disequilibrium of CO_2: Implications for the oceanic uptake of anthropogenic CO_2. *Geophysical Research Letters*, *28*, 555–558.

Herguera, J. C., Herbert, T., Kashgarian, M., & Charles, C. (2010). Intermediate and deep water mass distribution in the Pacific during the Last Glacial Maximum inferred from oxygen and carbon stable isotopes. *Quaternary Science Reviews*, *29*, 1228–1245.

Herguera, J. C., Jansen, E., & Berger, W. H. (1992). Evidence for a bathyal front at 2000-M depth in the glacial Pacific, based on a depth transect on Ontong-Java Plateau. *Paleoceanography*, *7*, 273–288.

Hertzberg, J. E., Lund, D. C., Schmittner, A., & Skrivanek, A. L. (2016). Evidence for a biological pump driver of atmospheric CO_2 rise during Heinrich Stadial 1. *Geophysical Research Letters*, *43*, 12,242–12,251. https://doi.org/10.1002/2016GL070723

Hoogakker, B. A. A., Lu, Z., Umling, N., Jones, L., Zhou, X., Rickaby, R. E. M., et al. (2018). Glacial expansion of oxygen-depleted seawater in the eastern tropical Pacific. *Nature*, *562*(7727), 410–413. https://doi.org/10.1038/s41586-018-0589-x

Hu, R., Noble, T. L., Piotrowski, A. M., McCave, I. N., Bostock, H. C., & Neil, H. L. (2016). Neodymium isotopic evidence for linked changes in Southeast Atlantic and Southwest Pacific circulation over the last 200 kyr. *Earth and Planetary Science Letters*, *455*, 106–114.

Jacobel, A. W., McManus, J. F., Anderson, R. F., & Winckler, G. (2017). Repeated storage of respired carbon in the equatorial Pacific Ocean over the last three glacial cycles. *Nature Communications*, *8*(1), 1727. https://doi.org/10.1038/s41467-017-01938-x

Key, R. M., Kozyr, A., Sabine, C. L., Lee, K., Wanninkhof, R., Bullister, J. L., et al. (2004). A global ocean carbon climatology: Results from Global Data Analysis Project (GLODAP). *Global Biogeochemical Cycles*, *18*, GB4031. https://doi.org/10.1029/2004GB002247

Knox, F., McElroy, M. B. (1984). Changes in atmospheric CO2 -Influence of the marine biota at high latitude. *Journal of Geophysical Research-Atmospheres*, *89*, 4629–4637.

Kroopnick, P. M. (1985). The distribution of C-13 of Sigma-CO_2 in the world oceans. *Deep-Sea Research Part a-Oceanographic Research Papers*, *32*, 57–84.

Lacerra, M., Lund, D., Gebbie, G., Oppo, D. W., Yu, J., Schmittner, A., & Umling, N. (2019). Less remineralized carbon in the intermediate-depth South Atlantic during Heinrich Stadial 1. *Paleoceanography and Paleoclimatology*, *34*, 1218–1233. https://doi.org/10.1029/2018PA003537

Lacerra, M., Lund, D., Yu, J., & Schmittner, A. (2017). Carbon storage in the mid-depth Atlantic during millennial-scale climate events. *Paleoceanography*, *32*, 780–795. https://doi.org/10.1002/2016PA003081

Lea, D. W., Bijma, J., Spero, H. J., & Archer, D. (1999). In G. Fischer, & G. Wefer (Eds.), *Implications of a carbonate ion effect on shell carbon and oxygen isotopes for glacial ocean conditions. Use of proxies in paleoceanography: Examples from the South Atlantic* (pp. 513–522). Berlin Heidelberg: Springer-Verlag.

Lueker, T. J., Dickson, A. G., & Keeling, C. D. (2000). Ocean pCO_2 calculated from dissolved inorganic carbon, alkalinity, and equations for K-1 and K-2: Validation based on laboratory measurements of CO_2 in gas and seawater at equilibrium. *Marine Chemistry*, *70*, 105–119.

Lund, D., Hertzberg, J., & Lacerra, M. (2019). Carbon isotope minima in the South Atlantic during the last deglaciation: Evaluating the influence of air-sea gas exchange. *Environmental Research Letters*, *14*.

Lund, D. C., Tessin, A. C., Hoffman, J. L., & Schmittner, A. (2015). Southwest Atlantic water mass evolution during the last deglaciation. *Paleoceanography*, *30*, 477–494. https://doi.org/10.1002/2014PA002657

Lynch-Stieglitz, J., Stocker, T., Broecker, W., & Fairbanks, R. G. (1995). The influence of air-sea exchange on the isotopic composition of oceanic carbon: Observations and modeling. *Global Biogeochemical Cycles*, *9*, 653–665.

Lynch-Stieglitz, J., Valley, S. G., & Schmidt, M. W. (2019). Temperature-dependent ocean-atmosphere equilibration of carbon isotopes in surface and intermediate waters over the deglaciation. *Earth and Planetary Science Letters*, *506*, 466–475.

Marchitto, T. M., Lynch-Stieglitz, J., & Hemming, S. R. (2005). Deep Pacific $CaCO_3$ compensation and glacial-interglacial atmospheric CO_2. *Earth and Planetary Science Letters*, *231*, 317–336.

Marcott, S. A., Bauska, T. K., Buizert, C., Steig, E. J., Rosen, J. L., Cuffey, K. M., et al. (2014). Centennial-scale changes in the global carbon cycle during the last deglaciation. *Nature*, *514*, 616–621.

Martin, J. H., Knauer, G. A., Karl, D. M., & Broenkow, W. W. (1987). VERTEX: Carbon cycling in the Northeast Pacific. *Deep-Sea Research Part a-Oceanographic Research Papers*, *34*, 267–285.

Martínez-García, A., Sigman, D. M., Ren, H. J., Anderson, R. F., Straub, M., Hodell, D. A., Jaccard, S. L., Eglinton, T. I., &Haug, G. H. (2014). Iron Fertilization of the SubantarcticOcean During the Last Ice Age. *Science*, *343*, 1347–1350.

Monnin, E., Indermühle, A., Dällenbach, A., Flückiger, J., Stauffer, B., Stocker, T. F., et al. (2001). Atmospheric CO_2 concentrations over the last glacial termination. *Science*, *291*(5501), 112–114. https://doi.org/10.1126/science.291.5501.112

Mook, W. G., Bommerson, J. C., & Staverman, W. H. (1974). Carbon isotope fractionation between dissolved bicarbonate and gaseous carbon-dioxide. *Earth and Planetary Science Letters*, *22*, 169–176.

Olsen, A., Key, R. M., van Heuven, S., Lauvset, S. K., Velo, A., Lin, X., et al. (2016). The Global Ocean Data Analysis Project version 2 (GLODAPv2): An internally consistent data product for the world ocean. *Earth System Science Data*, *8*(2), 297–323. https://doi.org/10.5194/essd-8-297-2016

Orsi, A. H., Johnson, G. C., & Bullister, J. L. (1999). Circulation, mixing, and production of Antarctic Bottom Water. *Progress in Oceanography*, *43*, 55–109.

Pahnke, K., & Zahn, R. (2005). Southern Hemisphere water mass conversion linked with North Atlantic climate variability. *Science*, *307*(5716), 1741–1746. https://doi.org/10.1126/science.1102163

Peterson, C. D., Lisiecki, L. E., & Stern, J. V. (2014). Deglacial whole-ocean delta C-13 change estimated from 480 benthic foraminiferal records. *Paleoceanography*, *29*, 549–563. https://doi.org/10.1002/2013PA002552

Putnam, A. E., Schaefer, J. M., Denton, G. H., Barrell, D. J. A., Andersen, B. G., Koffman, T. N. B., et al. (2013). Warming and glacier recession in the Rakaia valley, Southern Alps of New Zealand, during Heinrich Stadial 1. *Earth and Planetary Science Letters*, *382*, 98–110. https://doi.org/10.1016/j.epsl.2013.09.005

Rae, J. W. B., Burke, A., Robinson, L. F., Adkins, J. F., Chen, T., Cole, C., et al. (2018). CO_2 storage and release in the deep Southern Ocean on millennial to centennial timescales. *Nature*, *562*(7728), 569–573. https://doi.org/10.1038/s41586-018-0614-0

Rae, J. W. B., Foster, G. L., Schmidt, D. N., & Elliott, T. (2011). Boron isotopes and B/Ca in benthic foraminifera: Proxies for the deep ocean carbonate system. *Earth and Planetary Science Letters*, *302*, 403–413.

Reid, J. L. (1997). On the total geostrophic circulation of the Pacific Ocean: Flow patterns, tracers, and transports. *Progress in Oceanography*, *39*, 263–352.

Reimer, P. J., Bard, E., Bayliss, A., Beck, J. W., Blackwell, P. G., Ramsey, C. B., et al. (2013). INTCAL13 and MARINE13 radiocarbon age calibration curves 0–50,000 years Cal BP. *Radiocarbon*, *55*(4), 1869–1887. https://doi.org/10.2458/azu_js_rc.55.16947

Ronge, T. A., Steph, S., Tiedemann, R., Prange, M., Merkel, U., Nurnberg, D., & Kuhn, G. (2015). Pushing the boundaries: Glacial/interglacial variability of intermediate and deep waters in the southwest Pacific over the last 350,000 years. *Paleoceanography*, *30*, 23–38. https://doi.org/10.1002/2014PA002727

Ronge, T. A., Tiedemann, R., Lamy, F., Köhler, P., Alloway, B. V., De Pol-Holz, R., et al. (2016). Radiocarbon constraints on the extent and evolution of the South Pacific glacial carbon pool. *Nature Communications*, *7*.

Rosenthal, Y., Boyle, E. A., & Slowey, N. (1997). Temperature control on the incorporation of magnesium, strontium, fluorine, and cadmium into benthic foraminiferal shells from Little Bahama Bank: Prospects for thermocline paleoceanography. *Geochimica et Cosmochimica Acta*, *61*, 3633–3643.

Sabine, C.L., Feely, R.A., Gruber, N., Key, R.M., Lee, K., Bullister, J. L., et al. (2004). The oceanic sink for anthropogenic CO2. *Science*, *305*, 367–371.

Sarnthein, M., Schneider, B., & Grootes, P. M. (2013). Peak glacial C-14 ventilation ages suggest major draw-down of carbon into the abyssal ocean. *Climate of the Past*, *9*, 2595–2614.

Schlitzer, R., 2004: Ocean Data View.

Schmitt, J., Schneider, R., Elsig, J., Leuenberger, D., Lourantou, A., Chappellaz, J., et al. (2012). Carbon isotope constraints on the deglacial CO_2 rise from ice cores. *Science*, *336*(6082), 711–714. https://doi.org/10.1126/science.1217161

Schmittner, A., Gruber, N., Mix, A. C., Key, R. M., Tagliabue, A., & Westberry, T. K. (2013). Biology and air-sea gas exchange controls on the distribution of carbon isotope ratios (delta C-13) in the ocean. *Biogeosciences*, *10*, 5793–5816.

Shane, P., Sikes, E. L., & Guilderson, T. P. (2006). Tephra beds in deep-sea cores off northern New Zealand: Implications for the history of Taupo Volcanic Zone, Mayor Island and White Island volcanoes. *Journal of Volcanology and Geothermal Research*, *154*, 276–290.

Sikes, E. L., Allen, K. A., & Lund, D. C. (2017). Enhanced delta C-13 and delta O-18 differences between the South Atlantic and South Pacific during the last glaciation: The deep gateway hypothesis. *Paleoceanography*, *32*, 1000–1017. https://doi.org/10.1002/2017PA003118

Sikes, E. L., Cook, M. S., & Guilderson, T. P. (2016). Reduced deep ocean ventilation in the Southern Pacific Ocean during the last glaciation persisted into the deglaciation. *Earth and Planetary Science Letters*, *438*, 130–138.

Sikes, E. L., Elmore, A. C., Allen, K. A., Cook, M. S., & Guilderson, T. P. (2016). Glacial water mass structure and rapid delta O-18 and delta C-13 changes during the last glacial termination in the Southwest Pacific. *Earth and Planetary Science Letters*, *456*, 87–97.

Sikes, E. L., Samson, C. R., Guilderson, T. P., & Howard, W. R. (2000). Old radiocarbon ages in the southwest Pacific Ocean during the last glacial period and deglaciation. *Nature*, *405*(6786), 555–559. https://doi.org/10.1038/35014581

Skinner, L., McCave, I. N., Carter, L., Fallon, S., Scrivner, A. E., & Primeau, F. (2015). Reduced ventilation and enhanced magnitude of the deep Pacific carbon pool during the last glacial period. *Earth and Planetary Science Letters*, *411*, 45–52.

Stott, L. D., Harazin, K. M., & Krupinski, N. B. Q. (2019). Hydrothermal carbon release to the ocean and atmosphere from the eastern equatorial Pacific during the last glacial termination. *Environmental Research Letters*, *14*.

Studer, A. S., Sigman, D. M., Martinez-Garcia, A., Benz, V., Winckler, G., Kuhn, G., et al. (2015). Antarctic Zone nutrient conditions during the last two glacial cycles. *Paleoceanography*, *30*, 845–862.

Subhas, A. V., Adkins, J. F., Rollins, N. E., Naviaux, J., Erez, J., & Berelson, W. M. (2017). Catalysis and chemical mechanisms of calcite dissolution in seawater. *Proceedings of the National Academy of Sciences of the United States of America*, *114*, 8175–8180.

Swart, N. C., & Fyfe, J. C. (2012). Observed and simulated changes in the Southern Hemisphere surface westerly wind-stress. *Geophysical Research Letters*, *39*, L16711. https://doi.org/10.1029/2012GL052810

Takahashi, T., Sutherland, S. C., Sweeney, C., Poisson, A., Metzl, N., Tilbrook, B., et al. (2002). Global sea-air CO(2) flux based on climatological surface ocean pCO(2), and seasonal biological and temperature effects. *Deep-Sea Research Part Ii-Topical Studies in Oceanography*, *49*(9-10), 1601–1622. https://doi.org/10.1016/S0967-0645(02)00003-6

Takahashi, T., Sutherland, S. C., Wanninkhof, R., Sweeney, C., Feely, R. A., Chipman, D. W., et al. (2009). Climatological mean and decadal change in surface ocean pCO_2, and net sea-air CO_2 flux over the global oceans. *Deep-Sea Research Part Ii-Topical Studies in Oceanography*, *56*(8-10), 554–577. https://doi.org/10.1016/j.dsr2.2008.12.009

Talley, L. (2011). *Descriptive Physical Oceanography: An Introduction*, (6th ed.p. 555). London, UK: Elsevier.

Tamsitt, V., Drake, H. F., Morrison, A. K., Talley, L. D., Dufour, C. O., Gray, A. R., et al. (2017). Spiraling pathways of global deep waters to the surface of the Southern Ocean. *Nature Communications*, *8*(1), 172. https://doi.org/10.1038/s41467-017-00197-0

Toggweiler, J. R., & Russell, J. (2008). Ocean circulation in a warming climate. *Nature*, *451*(7176), 286–288. https://doi.org/10.1038/nature06590

Ullermann, J., Lamy, F., Ninnemann, U., Lembke-Jene, L., Gersonde, R., & Tiedemann, R. (2016). Pacific-Atlantic Circumpolar Deep Water coupling during the last 500 ka. *Paleoceanography*, *31*, 639–650. https://doi.org/10.1002/2016PA002932

Umling, N. E., Oppo, D. W., Chen, P., Yu, J., Liu, Z., Yan, M., et al. (2019). Atlantic circulation and ice sheet influences on upper South Atlantic temperature during the last deglaciation. *Paleoceanography and Paleoclimatology*, *34*, 990–1005. https://doi.org/10.1029/2019PA003558

Umling, N. E., & Thunell, R. C. (2018). Mid-depth respired carbon storage and oxygenation of the eastern equatorial Pacific over the last 25,000 years. *Quaternary Science Reviews*, *189*, 43–56.

Uppström, L. R. (1974). Boron/chlorinity ratio of deep-sea water from the Pacific Ocean. *Deep-Sea Research*, *21*, 161–162.

van Heuven, S., J. W. B. Rae, E. Lewis, and D. W. R. Wallace, 2011: MATLAB program developed for CO2 system calculations. O. R. N. ORNL/CDIAC-105b. Carbon Dioxide Information Analysis Center, and U. S. D. o. E. Laboratory, Eds.

Yu, J., & Elderfield, H. (2007). Benthic foraminiferal B/Ca ratios reflect deep water carbonate saturation state. *Earth and Planetary Science Letters*, *258*, 73–86.

Yu, J., Elderfield, H., & Piotrowski, A. M. (2008). Seawater carbonate ion-[delta]^{13}C systematics and application to glacial-interglacial North Atlantic ocean circulation. *Earth and Planetary Science Letters*, *271*, 209–220.

Yu, J., Menviel, L., Jin, Z. D., Thornalley, D. J. R., Foster, G. L., Rohling, E. J., et al. (2019). More efficient North Atlantic carbon pump during the Last Glacial Maximum. *Nature Communications*, *10*(1), 2170. https://doi.org/10.1038/s41467-019-10028-z

Yu, J. M., Anderson, R. F., Jin, Z. D., Menviel, L., Zhang, F., Ryerson, F. J., & Rohling, E. J. (2014). Deep South Atlantic carbonate chemistry and increased interocean deep water exchange during last deglaciation. *Quaternary Science Reviews*, *90*, 80–89.

Yu, J. M., Anderson, R. F., Jin, Z. D., Rae, J. W. B., Opdyke, B. N., & Eggins, S. M. (2013). Responses of the deep ocean carbonate system to carbon reorganization during the Last Glacial-interglacial cycle. *Quaternary Science Reviews*, *76*, 39–52.

Yu, J. M., Broecker, W. S., Elderfield, H., Jin, Z. D., McManus, J., & Zhang, F. (2010). Loss of carbon from the deep sea since the Last Glacial Maximum. *Science*, *330*(6007), 1084–1087. https://doi.org/10.1126/science.1193221

Zeebe, R. E., & Wolf-Gladrow, D. A. (2001). *CO2 in seawater: Equilibrium, kinetics, isotopes*, (Vol. 65, p. 346). London, UK: Elsevier.